Local Molecular Motion in Polyurethane–Poly(methyl methacrylate) Interpenetrating Polymer Networks

A. K. Rizos,*,†,‡ G. Fytas,‡ R. J. Ma,§ C. H. Wang,§ V. Abetz,∥ and G. C. Meyer⊥

Foundation for Research and Technology—Hellas, Heraklion 71110, Crete, Greece, Department of Chemistry, University of Nebraska—Lincoln, Lincoln, Nebraska 68588, Max-Planck-Institut für Polymerforschung, P.O. Box 3148, 6500 Mainz, Germany, and University Louis Pasteur, EAHP 67000 Strasbourg, France

Received September 29, 1992; Revised Manuscript Received January 29, 1993

ABSTRACT: Dynamic light scattering (photon correlation (PCS) and Brillouin spectroscopy (BS)) and dielectric relaxation (DS) techniques are employed to study local segmental motion in an interpenetrating polymer network (IPN) of poly(methyl methacrylate) (PMMA) with 50 wt % polyurethane (PUR) content and the constituent pure PMMA and PUR networks over the temperature (T) range from 140 to 410 K. For the PMMA network, the dielectric loss $\epsilon''(\omega)$ shows a strong secondary (β) relaxation, whereas dynamic light scattering arises from both β and primary (α) relaxation with characteristics very similar to the linear PMMA. The PUR network displays a relatively broad α-relaxation process in the PCS and DS experiments. The IPN exhibits two well-separated primary relaxation processes assigned to local regions of mobility distinguished by different degrees of mixing. β-Relaxation becomes faster in the IPN, indicating a reduced packing density. At high temperatures the fast α-relaxation process dominates the Brillouin spectra, leading to significant hypersonic attenuation. The hypersonic velocity shows an additional temperature kink characteristic of the upper high glass transition temperature due to the hard PMMA phase. The use of complementary techniques allows the dynamic study of the present IPN over a broad temperature and time range.

Introduction

Interpenetrating polymer networks (IPNs)[1,2] are incompatible polymer blends in which macroscopic phase separation is prevented through cross-linking of the constituent homopolymers. Their immiscibility is documented by the presence of two distinct glass transitions[4] if the length scale of the composition heterogeneities is longer than about 100 Å. The resolution of two separate glass transition temperatures (T_g) in IPNs is more difficult than that in corresponding physical blends. Instead, the glass transition in polyurethane (PUR)–poly(methyl methacrylate) (PMMA) IPNs occurs[3] over a very broad range of temperature. The high optical transmission of these IPNs is considerably affected by the extent of interpenetration, in contrast to the physical blends of PUR/PMMA which are opaque. In the case of optically transparent IPNs[3,4] the correlation length of the composition fluctuations is smaller than the wavelength of light. Therefore, it is interesting to study the molecular motion in local regions of these complex materials by spectroscopic techniques.

PMMA and the present PUR are isorefractive and yield therefore always transparent materials, when combined as in situ sequential (Seq) IPNs.[5] The presence of a more or less pronounced turbidity may have two origins: (a) unexpected defects in the PUR network (owing to free or pendant poly(oxypropylene glycol) (POPG) chains); (b) the IPNs obtained through another synthesis mode, e.g., in situ simultaneous (Sim) IPNs (both syntheses start simultaneously).

Despite the extensive technological relevance of IPNs, the characterization[3,4] of the material in the bulk state is mainly restricted to thermal and mechanical properties. As noticed earlier,[3] calorimetric measurements on PUR–PMMA IPN display broad glass transition features probably due to phase dispersion in the nanometer scale. Dynamic mechanical measurements on the same IPN are also limited because of the similar characteristics of the secondary (β) relaxation in pure PMMA and the corresponding transition in IPNs at low temperatures. However, the upper (higher-temperature) mechanical loss peak[4] owing to the primary (α) relaxation in the PMMA-rich phase is not subject to this limitation.

Dielectric spectroscopy (DS) has recently been performed, and it reveals various relaxation processes in these PUR–PMMA IPNs.[6] As expected from the dielectric spectrum of bulk PMMA, the dielectric loss ϵ'' in IPNs is dominated by the β relaxation of the PMMA component. The α-relaxation process in PUR local regions of IPNs cannot be resolved as a separate peak due to its relatively small dielectric strength. In a very recent nuclear magnetic resonance (NMR) study[7] on an in situ Seq IPN and in situ Sim IPN (25 wt % PUR), it was found that in the former the phase dispersion is high due to the already existing PUR network, which impedes from phase separation. A line-shape analysis has also indicated stronger interactions between the two components at high temperatures. Actually, PUR exerts a softening effect on PMMA, and vice versa.

Given the heterogeneous local structure of IPNs, the study of the molecular motions associated with relaxation processes in both PMMA and PUR microregions would provide a thorough characterization of these materials. Other experimental techniques that one can use to study local polymer dynamics have so far rarely been employed. In particular, dynamic light scattering (photon correlation (PCS) and Brillouin spectroscopy (BS)) techniques[8] can be used to investigate their dynamics over a broad range (10^3–10^{-11} s) in transparent polymeric systems.

We have employed for the first time the techniques of PCS and BS to investigate the segmental dynamics in a transparent 50 wt % PUR–PMMA IPN and corresponding cross-linked PMMA and PUR networks over a broad temperature range from 140 to 410 K. Preliminary light scattering results are reported elsewhere.[9] For comparison,

† Department of Chemistry, University of Crete, Heraklion 71110, Crete, Greece.
‡ Foundation for Research and Technology—Hellas.
§ University of Nebraska—Lincoln.
∥ Max-Planck-Institut für Polymerforschung.
⊥ University Louis Pasteur.

0024-9297/93/2226-1869$04.00/0

Table I
Materials

materials	description	source	code
polyol	poly(oxypropylene glycol): $\bar{M}_n$ = 2000; 1.05 OH/kg; density, 1.0 g/mL; viscosity, 370 cP	ARCO Chemical (ARCOL 1020)	POPG
polyisocyanate	trimethylol-1,1,1-propane/toluene diisocyanate adduct, containing 25 wt % of ethyl acetate: 3.1 NCO/kg; density, 1.17 g/mL	Bayer (L 75)	L 75
PUR catalyst	stannous octoate: 28.5% tin; density, 1.25 g/mL	Goldschmidt (KOSMOS 29)	OsSn
acrylic monomer	methyl methacrylate: stabilizer, hydroquinone (50 ppm)	Fluka	MAM
acrylic cross-linking agent	trimethylol-1,1,1-propane trimethacrylate: stabilizer methylhydroquinone (100 ppm); density, 1.06 g/mL	Degussa (TRIM)	TRIM
initiator	azobis(isobutyronitrile)	Merck	AIBN

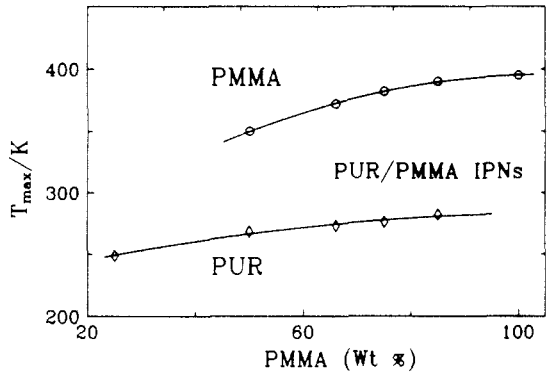

Figure 1. Composition variation of the two T_{max} at maximum mechanical loss for PUR-(◇) and PMMA-rich (○) regions of PUR–PMMA IPNs.

we have also measured the $\epsilon''(\omega)$ of the same samples over the frequency range 0.1–10^6 Hz; the dielectric spectrum of the PUR network is measured for the first time. The present results show phase separation in the nanometer scale. The α process associated with the PUR component within PUR-rich microregions becomes slower in the IPN due to some miscibility of PUR and PMMA components. More extensive mixing within PMMA-rich microregions is observed at higher temperatures in agreement with the NMR results.[7] The molecular motion involved in the β-relaxation dielectric loss peak is faster than that in the PMMA network, probably reflecting changes in the intermolecular barriers in the IPN. Two main glass transitions are present in the hypersonic speed in support of the mechanical results.

Experimental Section

Samples. An overview of the various materials is given in Table I. Water traces were eliminated, whereas the methacrylic monomers were not freed from the inhibitor molecules. A standard synthesis proceeds as follows: the calculated amounts of the various reagents are mixed and stirred thoroughly in a dry-nitrogen atmosphere for a few minutes. The homogeneous blend is poured into a glass mold. The PUR network is formed first at room temperature to complete conversion (~30 min in the present experimental conditions). Then, the mold is transferred to a heating oven at 60 °C, where the radical copolymerization of the acrylic phase is initiated. After 1 h at 60 °C, the temperature is raised to 75 °C for 1 night, and the annealing is finished by heating at 120 °C for 2 h. Such a procedure (homogeneous blending of all the reagents involved and sequential synthesis of the two networks) yields the so-called in situ sequential 50 wt % PUR–PMMA (Seq) IPN. Cylindrical rods (10 mm) and films with a thickness of 50 μm and a diameter of 20 mm were prepared respectively for the light scattering and DS experiments. Dynamic mechanical measurements[4] of 0.1 rad/s have revealed a strong and broad high-temperature (upper) transition and a weaker (lower) transition. Figure 1 displays the temperature T_{max} at maximum tan δ loss at a frequency of 0.1 rad/s.

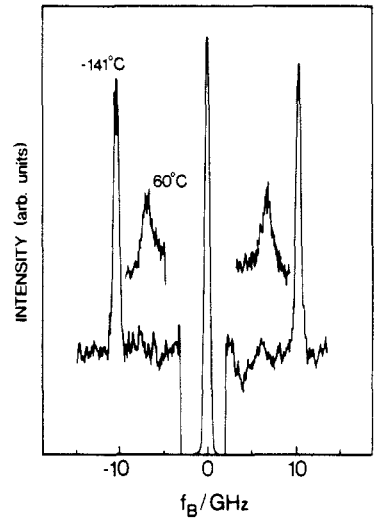

Figure 2. Polarized Rayleigh–Brillouin spectra for the 50/50 PUR–PMMA IPN at 333 and 132 K.

Dynamic Light Scattering. The correlation function of the depolarized light scattering intensity $G_{VH}(t)$ over 8 decades in time was measured with an ALV5000 digital correlator at a scattering angle of 90°, in the temperature range between 255 and 398 K. Due to the high polarized light scattering intensity of the present 50 wt % PUR–PMMA IPN sample, we have measured only $G_{VH}(t)$. The light source was an Ar^+ laser (Spectra Physics 2020) operating at 488-nm wavelength with a power of 150 mW. The incident beam was polarized vertically (V) with respect to the scattering plane, and the scattered light intensity from the sample was collected through a Glan–Thompson polarizer with an extinction coefficient better than 10^{-7}. The scattered light was polarized horizontally (H) to the scattering plane. Assuming ergodicity, the desired correlation function $C(t) = [G_{VH}(t)/A - 1]^{1/2}$, with A being the base line.

Rayleigh–Brillouin spectra were obtained in the VV scattering configuration at a scattering angle of 90° using a piezoelectrically scanned five-pass Fabry–Perot interferometer (FPI) in the temperature range from 140 to 390 K. The shift ω_B and line width $2\Gamma_B$ of the Brillouin doublet were obtained from the fit of the Brillouin peaks to a Lorentzian line shape in the region not affected by the central Rayleigh peak. To correct $2\Gamma_B$ for the instrumental broadening, the instrumental width was subtracted from the measured line width of the Brillouin line. Figure 2 shows the Rayleigh–Brillouin spectra of the IPN at 333 and 132 K.

Dielectric Spectroscopy (DS). The real and imaginary parts of the complex dielectric permitivity ϵ'' were measured from 10^{-1} to 10^6 by using a Solartron–Schlumberger frequency analyzer FRA-1260. The sample was kept between the gold-plated stainless steel electrodes, and the temperature was varied from 203 up to 423 K.

Data Analysis and Results

The time correlation function $C(t)$ of the IPN sample near the lower T_g is considerably broader than that of the cross-linked PUR component. Figure 3 shows this com-

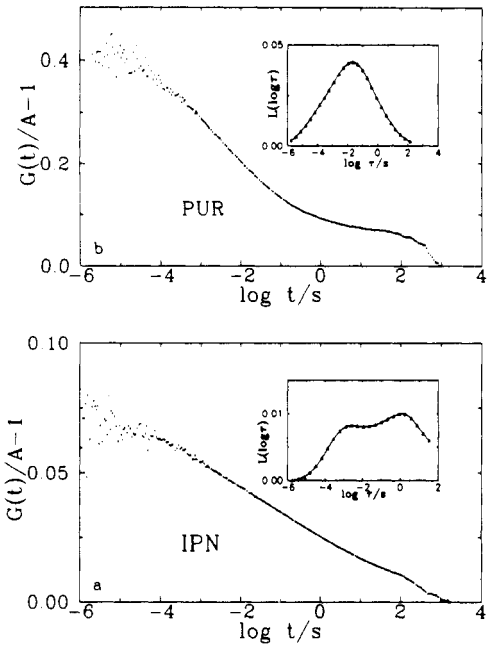

Figure 3. Depolarized intensity autocorrelation functions at 258 K for (a) a 50/50 PUR-PMMA IPN (and (b) a PUR network. The distributions of retardation times $L(\log \tau)$ are included as insets. The extra peak in $L(\log \tau)$ due to the slow decay of $C(t)$ at $t > 100$ s is omitted for both samples.

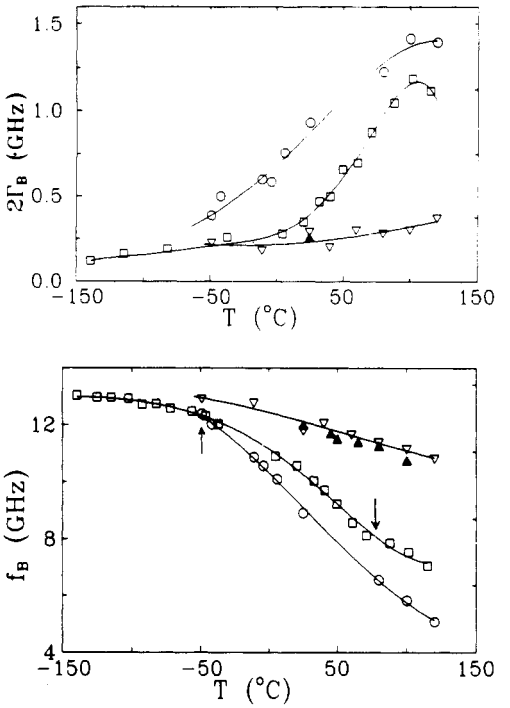

Figure 4. Brillouin shift f_B and line width $2\Gamma_B$ for 50/50 PUR-PMMA IPN (□), crosslinked PMMA (▽), linear PMMA (▲), and PUR (○) plotted as a function of temperature.

parison for the depolarized intensity autocorrelation function at 258 K. An intensive slow mode is present in the $C(t)$, but its origin remains to be elucidated. The lower amplitude of $C(t)$ for the IPN sample is probably caused by the presence of both fast ($t < 10^{-6}$ s) dynamic and slow static light scattering contributions to the total light scattering intensity. The former arises from fast orientation fluctuations of the PUR component, whereas the most important ultraslow ($t > 100$ s) fluctuations originate from PMMA and PUR hindered by the PMMA[7] motions. The measured intensity autocorrelation functions have routinely been fitted to the Kohlrausch-Williams-Watts (KWW) expression $\exp[-(t/\tau)^\beta]$ which yields the relaxation time τ and the distribution parameter β. The shape parameter β assumes respectively the values 0.15 and 0.26 for the IPN and PUR homonetwork.

Due to deviations from the KWW fit we have carried out the inverse Laplace transformation (ILT) of the time correlation functions without assumption of the shape of the underlying distribution function $L(\ln \tau)$ but assuming a superposition of exponentials.

$$C(t) = \int_{-\infty}^{\infty} L(\ln \tau) \exp(-t/\tau)\, \mathrm{d} \ln \tau \qquad (1)$$

In this manner the nonexponentiality is taken into account in terms of a continuous spectrum of relaxation times $L(\ln \tau)$. For the time correlation functions of Figure 3, the relaxation distribution function $L(\log \tau)$ for $\tau < 100$ s is shown in the same figure. It is worth noting the broad but single peak in PUR and the dual character of $L(\log \tau)$ in the IPN. For the latter, the two peaks can be assigned to the α relaxation within PUR-rich regions and the faster β mode due to the PMMA component.

In the Brillouin experiment (BS)[6] light is scattered by thermally induced acoustic waves in the sample. The BS spectrum is determined by the frequency dependence of the dynamic longitudinal modulus $M^*(\omega)$ at hypersonic frequencies. The Brillouin shift f_B ($=\omega_B/2\pi$) is associated with the storage modulus M' whereas the line width $2\Gamma_B$ (full width at half-height) is proportional to the loss modulus M''. In viscoelastic fluids the main source for hypersonic dispersion is the primary (α) glass-rubber relaxation. In this case, $2\Gamma_B$ exhibits a maximum at a temperature T_{max} for which $\omega_B \tau \simeq 1$. Thus, in contrast to PCS, BS allows the determination of τ in the picosecond range and hence at high temperatures far above T_g.

The Brillouin shift f_B and line width $2\Gamma_B$ for the 50/50 PUR-PMMA IPN and the corresponding homonetworks are plotted as a function of temperature in Figure 4. For the PUR network and IPN, the hypersonic attenuation appears to attain its maximum value at about 378 K. The structural relaxation time τ amounts then to 4×10^{-11} s respectively for both PUR and IPN. As expected from the T_g value of bulk PMMA, the $2\Gamma_B$ of the PMMA network should attain its maximum at much higher temperatures. In fact, the T_{max} of maximum $2\Gamma_B$ for linear-chain PMMA[11] is very high (≈550 K). On the basis of the latter observation and the closeness between the T_{max} values of IPN and the PUR network, the hypersonic attenuation maximum in the IPN is ascribed to molecular motion within the PUR-rich region. The variation of f_B with temperature will be discussed in the next section.

The dielectric response of the present IPN originates from the permanent dipole moments in both components. Like the situation in linear-chain PMMA, the $\epsilon''(\omega)$ of cross-linked PMMA is dominated by the strong β relaxation whereas the contribution of the α process is very weak. The situation is illustrated in Figure 5a. The $\epsilon''(\omega)$ spectrum becomes broader and the peak position shifts at a moderate rate to lower frequencies with decreasing temperature below T_g. It is therefore anticipated that the $\epsilon''(\omega)$ spectrum of the locally heterogeneous IPN sample will resemble the $\epsilon''(\omega)$ of Figure 5c at low temperatures and $\epsilon''(\omega)$ of Figure 5a at high temperatures. For the IPN, the dielectric loss is plotted versus frequency in Figure 5b and is in agreement with the recently reported[6] $\epsilon(T)$ of the same sample at 1 kHz. For the well-defined β relaxation in pure PMMA and IPN, the experimental $\epsilon(\omega)$ can be represented by a single Havriliak-Negami (HN)[12] function

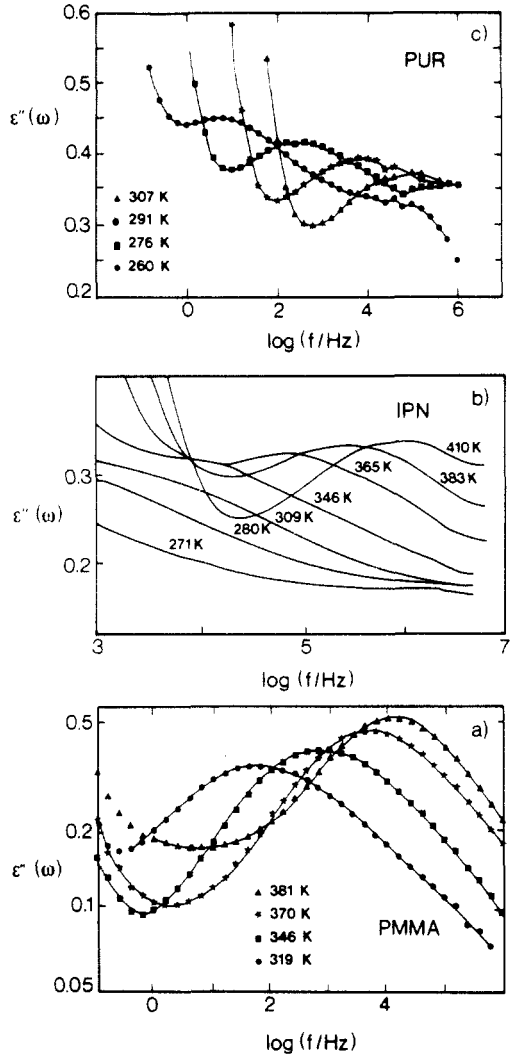

Figure 5. Dielectric loss ϵ'' vs frequency for cross-linked PMMA (a), 50/50 PUR–PMMA IPN (b), and PUR (c), at different temperatures.

$$\epsilon^* - \epsilon_\infty = \Delta\epsilon/[1 + (i\omega\tau)^\alpha]^\gamma \qquad (2)$$

plus a conductivity term to extract the characteristic relaxation parameters.[13] Here, ϵ_∞ is the high-frequency limiting value of ϵ, and α and γ are parameters ($0 \leq \alpha, \gamma \leq 1$) describing respectively the symmetric and asymmetric broadening of the distribution. For cross-linked PMMA a single HN function was adequate to represent $\epsilon''(\omega)$, and these parameters assume the values of $\gamma = 0.73$ and α varies between 0.54 and 0.32 at 381 and 290 K, respectively. By following a standard procedure,[13] namely, the KWW fit to the Fourier transform of the DS data, we obtain the time-domain relaxation function with a KWW $\beta = 0.45$–0.31. The HN parameters for the present IPN assume the values of $\alpha = 0.32$–0.51 and $\gamma = 0.55$–0.78 over the T range between 410 and 365 K for which a single HN function could fit the experimental $\epsilon''(\omega)$. The time-domain transformation gives virtually a T independent β value of 0.29.

Discussion

Near T_g a characteristic correlation length ξ ($\sim$2 nm) can be assigned to the primary (α) relaxation of viscoelastic media.[14] Compositional heterogeneities within these subvolumes can lead to two distinct primary time scales in the macroscopically homogeneous system exhibiting a single calorimetric glass transition.[15]

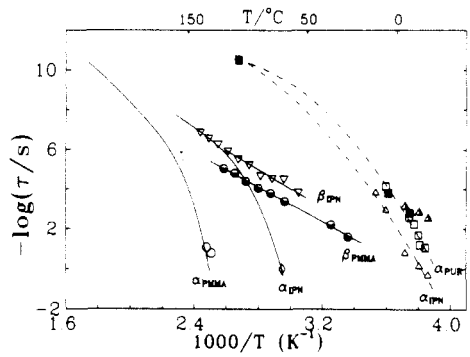

Figure 6. Temperature dependence of the retardation times obtained by different techniques: PCS for 50/50 IPN (△, ▲); BS for 50/50 IPN (▲); DS for 50/50 IPN (▽); MR for 50/50 IPN (◇); PCS for PUR (□); BS for PUR (◪); DS for PUR (■); PCS for cross-linked PMMA (○); DS for cross-linked PMMA (◒). For the α process dashed lines denote the fit of eq 4 to the experimental times whereas the solid lines are computed from ref-chain 9. For the β process in PMMA, the solid line represents the β relaxation times for linear-chain (un-cross-linked) PMMA.[11]

For the present IPN,[3] calorimetry can hardly reveal well-separated T_g's, in contrast to the physical blends of PUR–PMMA. Conversely, dynamic mechanical measurements show a strong α peak at temperatures near and below the T_g of the PMMA homopolymer, but the lower transition at temperatures near the T_g of the PUR component cannot be unequivocally assigned.

Alternatively, DS of the present IPN is dominated by the secondary β relaxation of the PMMA component. The present PCS and BS measurements, however, probe a fast relaxation process which resembles the α mode of the PUR component. On the basis of the light scattering and mechanical results, there is strong evidence that the PUR–PMMA IPN exhibits two main microregions characterized by vastly separated segmental mobilities. Knowledge of the relaxational characteristics will help elucidate the material structure within these microphases.

High-Mobility Region. First, we should mention the broad $L(\log \tau)$ distribution function in the PUR homonetwork. Earlier PCS measurements[16] in bulk POPG have revealed a significantly narrower distribution function characterized by $\beta \simeq 0.4$. The significantly lower β (=0.26) for PUR results probably from dynamical heterogeneities due to motions of isocyanate cross-linking agent, rigidified[7] (near the cross-link points) and mobile POPG segments.

Both IPN and PUR networks exhibit dynamic light scattering over a similar T range. Similar relaxation times are therefore obtained from PCS at low T near the lower T_g and BS at T about 120 K higher. At these T's, the segmental dynamics of PMMA homopolymer is practically frozen and contributes only to static light scattering. Near the lower T_g, the time correlation functions of the IPN are considerably broader as compared to the pure PUR network (Figure 3). As it can be inferred from the inset of Figure 3a, the broader shape of $C(t)$ results from the two-peak structure of the $L(\log \tau)$. On the basis of the temperature dependence, the slow peak can be assigned to the α relaxation of PUR whereas the less temperature-dependent fast peak probably originates from the β-relaxation process in the IPN. In fact, the presence of β relaxation in $L(\log \tau)$ was reported[11] for linear-chain PMMA and also found in the present cross-linked PMMA (Figure 6). Thus the relaxation times τ_f for the fast α process obtained from the slow peak of $L(\log \tau)$ in Figure 3 characterize mobile regions in the IPN. However, these regions are not in pure PUR phases. The observed slowing down of τ_f in the IPN indicates partial miscibility. A rough

estimate of the PUR weight fraction w_1 in the mobile regions is obtained from the known miscibility relation

$$1/T_{1/2} = w_1/T_1 + w_2/T_2 \quad (3)$$

where $T_{1,2}$ and T_1 and T_2 are respectively isochrones for IPN and pure PUR and PMMA networks. Using T_1 = 254 K, T_2 = 400 K, and $T_{1,2}$ = 259 K for a relaxation rate of 1 Hz (Figure 6), the PUR weight percent in the high-mobility region is about 95%. Apart from the uncertainties involved, such a high value should be expected for strongly incompatible components. For a 25 wt % PUR–PMMA Seq-IPN[7] at low T, the analysis of the solid-state ^{1}H NMR has required a lower fraction of mobile PUR than expected for an incompatible PUR–PMMA mixture. This reduced PUR mobility was assigned to interactions between the components involving partial mixing. The model-dependent line-shape analysis is therefore in qualitative agreement with the present PCS results.

The relaxational characteristics (i.e., average time and width of the distribution in the high-mobility region corresponding to the PUR component) should be influenced by the vitrification of the low-mobility PMMA network. Annealing near the upper T_g affects the glassy structure of the hard component and is therefore expected to alter the segmental relaxation of the soft component in the rubbery state. Spatial heterogeneity and hence the breadth of the distribution of the fast segmental times is expected to be affected by physical aging. PCS can be employed to reveal this effect; albeit the contribution of the β relaxation might complicate the picture.

Several experimental findings emerge from the Brillouin experiment. (i) The maximum hypersonic absorption ($\sim 2\Gamma_B$) in the IPN occurs at roughly the same T as in the pure network. (ii) At low T's, $2\Gamma_B$ of the IPN has a value comparable to the pure components (Figure 4). (iii) The hypersonic velocity ($\sim f_B$) decreases with increasing PUR content, and for the IPN it displays an interesting new feature; its T-dependence exhibits two kinks at about −50 and +80 °C. (iv) Below about −50 °C, all networks assume very similar f_B values.

All these findings suggest that the hypersonic dispersion can be assigned as due to local structural rearrangements within microregions rich in PUR. In the vicinity of the lower T_g, compressibility and density of the IPN changes cause the first kink in $f_B(T)$ (arrow in Figure 4). At lower T, all materials are in the glassy state with apparently similar free volume values (f_g) and hence hypersonic speed. Above the lower T_g, the dispersion in the Brillouin f_B and $2\Gamma_B$ is mainly determined by the rubbery state of the soft PUR component. Upon the addition of PUR, f_B decreases whereas $2\Gamma_B$ increases. The rate of decrease in f_B with increasing T shows a second change at about 80 °C. This second kink as indicated by an arrow in Figure 4 signals the effect of the upper T_g of the hard phase rich in PMMA. In this context we should also note that f_B in the present IPN displays behavior similar to that of PUR and furthermore assumes a value closer to f_B of the PUR homonetwork with the lower rigidity. In contrast compatible polymer blends of PMMA/poly(ethylene oxide)[15] have shown rigidity similar to the PMMA network. Moreover, cross-linking leads to slightly higher f_B and hence a corresponding increase in the elastic modulus as indicated by the experimental values of linear-chain (▲) and cross-linked PMMA (▽).

The relaxation time $\tau = 1/\omega_B$ at T_{max} at which $2\Gamma_B$ exhibits a maximum value in the IPN and PUR network is shown by an Arrhenius plot in Figure 6. The relaxation time τ_f corresponding to the maximum of $L(\log \tau)$ (Figure 3) and the maximum mechanical tan δ in IPN[3] are also plotted in Figure 6. The strong T dependence of τ_f is characteristic of an α-relaxation process. Apart from the difference between structural relaxation times obtained at low T by PCS and at high T by BS,[17] to encompass a larger T range, we have used the Vogel–Fulcher–Hesse–Tamman (VFHT) temperature equation:

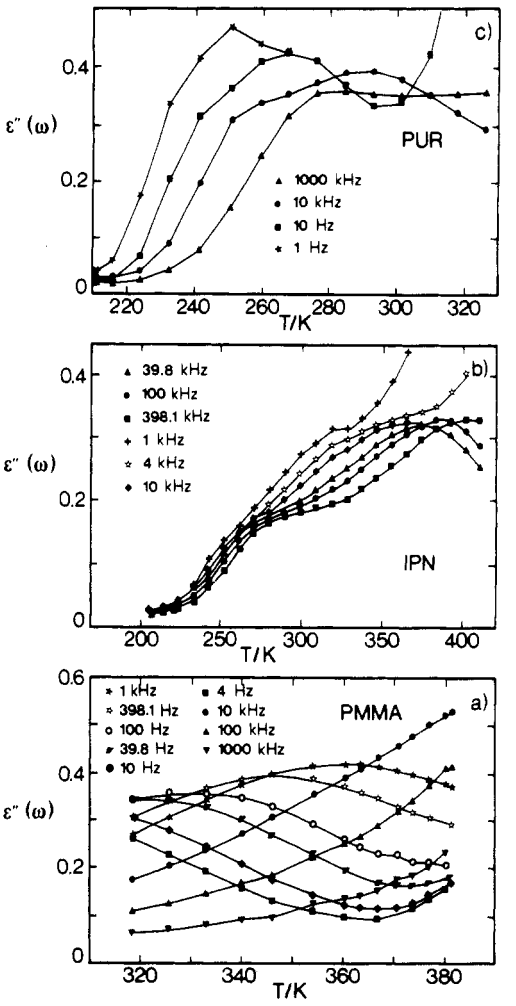

Figure 7. Isochrones ϵ'' for cross-linked PMMA (a), 50/50 PUR–PMMA IPN (b), and PUR (c) constructed from the $\epsilon''(\omega)$ (Figure 5) at certain frequencies.

$$\tau = \tau_0 \exp[B/(T - T_0)] \quad (4)$$

to fit all experimental times in PUR-rich microregions. For IPN, we obtain a limiting high T value $\tau_0 = 2.3 \times 10^{-13}$ s, the activation parameter B = 1260 K, and the ideal glass transition temperature T_0 = 210 K. For comparison, these parameters in the pure PUR network assume the values $\tau_0 = 3.2 \times 10^{-13}$ s, B = 1103 K, and T_0 = 218 K. The similarities in the τ_0 and B values for IPN and PUR are in accord with the high PUR content within soft microregions of the former. The relaxational behavior in the high-mobility regions supports the weak composition variation of the lower mechanical T_{max} data of Figure 1. Moreover, the activation parameter B is similar to that in bulk POPG.[16]

The dielectric measurements on the PUR homonetwork reveal (Figures 5 and 7) the α relaxation of PUR in accordance with the PCS results as well as a fast mode around 275 K (Figure 7) which is also present in the IPN network. This dielectrically active process cannot be associated with the PMMA network since it is not observed there. Obviously, this fast relaxation process is associated

with motions much faster than those of the β process of PMMA.

Low-Mobility Region. The second kink in $f_B(T)$ of the IPN at about 80 °C indicates a higher T_g associated with the PMMA network. Additional evidence originates from the T_{max} of maximum mechanical tan δ (Figure 1). In this context, we should mention that the manifestation of the glass transition in the shift f_B occurs somewhat below the calorimetric T_g due to the usually slower T variation of the Brillouin experiment. The primary (○) as well as the secondary (◒) relaxation times of the PMMA network are shown in Figure 6. For the IPN, only one (mechanical) (◇) data point is displayed. Due to the domination of the β-relaxation process and the extremely broad shape of time correlation functions, PCS data in this T range cannot be uniquely analyzed. Since the primary process is insensitive to molecular weight and cross-linking, we have included for comparison the segmental relaxation times of a linear PMMA polymer[11] ($M_w = 1 \times 10^7$) (solid line in Figure 6).

For the pure PMMA linear-chain component, the fit of VFHT equation (4) yields $\tau_0 = 3.2 \times 10^{-13}$ s, $B = 1480$ K, and $T_0 = 347$ K. It is worth noting that the activation parameter B is larger in PMMA than in PUR networks. A pertinent aspect of the slow α-relaxation time τ_s in IPN (Figure 6) is its stronger composition dependence than that of τ_f. This variation can be rationalized by assuming enhanced miscibility in the hard microphase at high T. In fact, an application of eq 3 leads to a 83 wt % PMMA content in the low-mobility region compared to the 95 wt % PUR composition in the soft phase. Higher mixing within PMMA-rich microregions of a 25 wt % PUR–Seq IPN was also very recently deduced from the ^{1}H NMR line-shape analysis.[7] The difference between the fractions of the mobile component in the IPN and the corresponding incompatible blend of the networks is an increasing function of T. This composition variation could, in principle, arise from a T-dependent interaction parameter χ and differences in the cooperative size[14] (ξ) for segmental rearrangements in the two regions. For the size of ξ, it can only be speculated that $\xi_{PUR} \leq \xi_{PMMA}$, which would, in principle, lead to a lower space resolution and hence an effectively lower PMMA content. Nevertheless, for the present Seq IPN the formation first of the PUR network seems to imply large miscibility within PMMA-rich microregions.

Secondary (β) Relaxation. Regarding the dielectric loss of IPN, the contribution of the β relaxation can easily be recognized. In the pure PMMA network near and below T_g, the β process dominates the experimental $\epsilon''(\omega)$. Figure 7 shows isochrones for the three samples. They are constructed from the isothermal $\epsilon''(\omega)$ (Figure 5) at particular frequencies. The characteristic relaxation times $\tau_B = 1/(2\pi f_{max})$ from the frequency at maximum loss are shown in the Arrhenius plot of Figure 6. As a comparison we have also plotted (solid line) the β-relaxation times of linear-chain (un-cross-linked) PMMA.

Since pure PMMA exhibits an intense β-relaxation peak, the secondary process in the IPN probably arises from motions within the PMMA-rich region. Similar to the assignment of PMMA, motions responsible for secondary dielectric activity in IPN are associated with the rotation of the ester (–$COOCH_3$) group and parts of the polymer chain.[18] The molecular motions involved in secondary relaxation of amorphous glassy polymers are also affected by physical aging which diminishes the average free volume of the glass. Thermal annealing[6,19] reduces the strength $\Delta\epsilon_\beta$ of the β process, whereas it has a minor effect on the relaxation time τ_β. This is an indication of the densification of amorophous polymers near T_g which reduces the number of molecular moieties responsible for secondary activity, while the intramolecular potentials and hence τ_β remain unchanged on annealing.

Secondary relaxation (▽ in Figure 6) is faster in IPN than in linear-chain (un-cross-linked) and cross-linked PMMA (◒). In fact, the longest τ_β are observed in the latter system. Using the experience for the amorphous bulk polymers, these findings suggest that the PMMA-rich region in the IPN experiences a somewhat lower potential energy barrier than in the pure PMMA network. In fact, the Arrhenius activation energy of τ_β is somewhat lower in the IPN ($E_\beta = 18 \pm 2$ kcal/mol) than in the cross-linked PMMA ($E_\beta = 20$ kcal/mol). The even higher value of E_β recently reported for the PMMA network[6] might be due to the influence of the α relaxation, since measurements were performed at T above the higher T_g of the IPN. The comparable strength $\Delta\epsilon_\beta$ in the IPN and cross-linked PMMA as obtained from the HN fit (eq 2) corroborates also the notion that the PMMA-rich regions in the IPN are less tightly packed. This local structure is in accordance with higher mixing within PMMA-rich regions, as discussed in the preceding section.

The secondary relaxation times (▽) of the present IPN are characterized by smaller α and γ HN fit values (as well as broader β KWW values of the corresponding time-domain relaxation function) as compared to cross-linked PMMA. The increase in β with increasing temperature is also seen in linear PMMA and has been attributed to the merging of α and β relaxations. The distribution parameter β for the secondary relaxation of PMMA in the present IPN is broad ($\beta = 0.27$–0.32) compared to the PMMA homonetwork ($\beta = 0.45$–0.31). In IPN each dipole in the side ester (–$COOCH_3$) group is surrounded by a different environment[19] in comparison to cross-linked PMMA and will, therefore, experience different potential energy barriers to rotation. This diversity of barriers is expected to yield a greater distribution of relaxation times and hence may be responsible for a smaller β value of the β relaxation in the IPN.

Concluding Remarks

The local molecular motion in a 50/50 Seq IPN of PMMA–PUR has been studied by dynamic light scattering (PCS and FPI) and dielectric relaxation techniques. The homonetwork and linear-chain (un-cross-linked) PMMA show similar features, whereas the PUR homonetwork displays broad α-relaxation processes in PCS and broad $\epsilon''(\omega)$ in the DS experiment. The IPN sample exhibits two well-separated α-relaxation processes attributed to regions of vastly different mobilities, characterized by different degrees of mixing at low and high T. The secondary β relaxation dominates the dielectric response and contributes to the dynamic light scattering intensity of IPN. The β mode is due to PMMA, and it becomes faster in the IPN probably due to the different energy landscape of the latter. The local heterogeneous nature of the IPN is also manifested in the temperature dependence of the hypersonic velocity.

Acknowledgment. We thank Dr. F. Kremer for providing us the dielectric instrument. C.H.W. acknowledges partial financial support of ONR and NSF (DMR 9-112993).

References and Notes

(1) Sperling, L. H. *Interpenetrating Polymer Networks and Related Materials*; Plenum: New York, 1981.

(2) Kempler, D.; Frisch, K. C. *Polymer Alloys II*; Plenum: New York, 1980.
(3) Hermant, I.; Damyandiu, M.; Meyer, G. C. *Polymer* **1983**, *24*, 1419.
(4) Djomo, H.; Morin, A.; Damyanidu, M.; Meyer, G. C. *Polymer* **1983**, *24*, 65.
(5) Tabka, M. T.; Widmaier, J. M.; Meyer, G. C. In *Sound and Vibration Damping with Polymers*; Corsaro, R. D., Sperling, L. H., Eds.; American Chemical Society: Washington, DC, 1990; p 445.
(6) Mai, C.; Johari, G. P. *J. Polym. Sci., Polym. Phys. Ed.* **1987**, *25B*, 1903.
(7) Parizel, N.; Meyer, G. C.; Weill, G. *Polymer* **1993**.
(8) Fytas, G.; Meier, G.; Patkowski, A. *Dynamic Light Scattering*; Brown, W., Ed.; Oxford Press: 1992; Oxford, U.K., Chapters 9 and 10.
(9) Rizos, A. K.; Fytas, G.; Wang, C. H.; Meyer, G. C. *Colloid Polym. Sci.* **1992**.
(10) Tabka, M. T.; Widmaier, J. M.; Meyer, G. C. *Macromolecules* **1989**, *22*, 1826.
(11) Fytas, G.; Wang, C. H.; Fischer, E. W. *Macromolecules* **1988**, *21*, 2253.
(12) Havriliak, S.; Negami, S. *Polymer* **1967**, *8*, 161.
(13) Böse, D.; Momper, B.; Meier, G.; Kremer, F.; Hagenah, J. U.; Fischer, E. W. *Macromolecules* **1989**, *22*, 4416.
(14) Fischer, E. W.; Donth, E.; Steffen, W. *Phys. Rev. Lett.* **1992**, *68*, 2344 and references therein.
(15) Fytas, G.; Kanetakis, J.; Floudas, G.; Wang, C. H. *Polym. Commun.* **1990**, *31*, 434.
(16) Wang, C. H.; Fytas, G.; Lielge, D.; Dorfmüller, Th. *Macromolecules* **1981**, *14*, 1363.
(17) Floudas, G.; Higgins, J. S.; Fytas, G. *J. Chem. Phys.* **1992**, *96*, 7672.
(18) Heijboer, J.; Baas, J. M. A.; van de Graaf, B.; Hoefnagel, M. A. *Polymer* **1987**, *28*, 509.
(19) Fischer, E. W.; Hellman, G. P.; Spiess, H. W.; Hörth, F. J.; Ecarius, U.; Wehle, M.; *Makromol. Chem., Suppl.* **1985**, *12*, 189.